SAND2007-6753C

Detailed HCCI Exhaust Speciation and the Sources of Hydrocarbon and Oxygenated Hydrocarbon Emissions

John E. Dec*, M. Lee Davisson‡, Magnus Sjöberg*, Roald N. Leif‡, and Wontae Hwang*

*Sandia National Laboratories

‡Lawrence Livermore National Laboratory

ABSTRACT

Detailed exhaust speciation measurements were made on an HCCI engine fueled with iso-octane over a range of fueling rates, and over a range of fuel-stratification levels. Fully premixed fueling was used for the fueling sweep. This sweep extended from a fuel/air equivalence ratio (ϕ) of 0.28, which is sufficiently high to achieve a combustion efficiency of 96%, down to a below-idle fueling rate of ϕ = 0.08, with a combustion efficiency of only 55%. The stratification sweep was conducted at an idle fueling rate, using an 8-hole GDI injector to vary stratification from well-mixed conditions for an early start of injection (SOI) (40°CA) to highly stratified conditions for an SOI well up the compression stroke (325°CA, 35°bTDC-compression). The engine speed was 1200 rpm.

At each operating condition, exhaust samples were collected and analyzed by GC-FID for the C1 and C2 hydrocarbon (HC) species and by GC-MS for all other species except formaldehyde and acetaldehyde. These two species were analyzed using high-performance liquid chromatography. In addition, standard emissions-bench exhaust analysis equipment was used to measure total HC, CO, CO_2, O_2, and NO_X simultaneously with the sampling for the detailed-speciation analysis. Good overall agreement was found between the emissions-bench data and total HC from the detailed measurements.

Unreacted fuel, iso-octane, was by far the most prevalent HC species at all operating conditions. Numerous other HC and oxygenated HC (OHC) species were found that could be identified as breakdown products of iso-octane. Several smaller HC and OHC species were also identified. At the highest ϕ, emissions of all species were low, except iso-octane. As ϕ was reduced, emissions of all species increased, but the rate of increase varied substantially for the different species. Analysis showed that these differences were related to the degree of breakdown from the parent fuel and the in-cylinder location where they formed. SOI-sweep results indicated that stratification improves combustion efficiency by reducing the fuel penetration to the crevice and cylinder-wall boundary-layer regions, as well as by creating a locally richer mixture that burns hotter and more completely.

INTRODUCTION

Homogeneous charge compression ignition (HCCI) engines are being widely investigated because they can provide both high diesel-like efficiencies and ultra-low nitrogen oxide (NO_X) and particulate emissions. However, there are several technical challenges that must be overcome before this promising technology is commercially viable. One significant challenge is that HCCI engines produce emissions of unburned hydrocarbons (HC), oxygenated hydrocarbons (OHC), and carbon-monoxide (CO) [1-4]. These emissions become particularly high at low loads, with a commensurate drop in the combustion efficiency to unacceptably low levels [3-5]. Research has shown that mixture stratification can increase low-load combustion efficiency substantially [3,6], and in a recent work, the authors showed that improved stratification could produce combustion efficiencies at idle that were only a few percent less than those for high loads [7]. Despite these improvements, however, aftertreatment will almost certainly still be required at all loads to control these HC, OHC, and CO emissions.

Although HC emissions have been measured since the early investigations of HCCI combustion [1,2], information on the individual species comprising these emissions is scant. This is because HC emissions are typically measured with an exhaust analyzer that measures the total carbon in the exhaust HC, but gives no information on species composition. Moreover, these HC analyzers use a flame ionization detector (FID), which is not sensitive to carbon atoms that are bound to oxygen. Therefore, OHC compounds give a reduced signal, or give no signal at all for species like formaldehyde, which have only one carbon atom that is bound to an oxygen atom. As a result, the presence of OHC compounds was not noted until more recently [8-10].

Before discussing the behavior of individual HC and OHC species, it is important to understand the primary sources of HC and OHC emissions and how their amounts are affected by operating condition. Figure 1 shows the trends of combustion efficiency and emissions plotted as a function of fuel/air equivalence ratio (ϕ) for operation with a fully premixed intake mixture of iso-

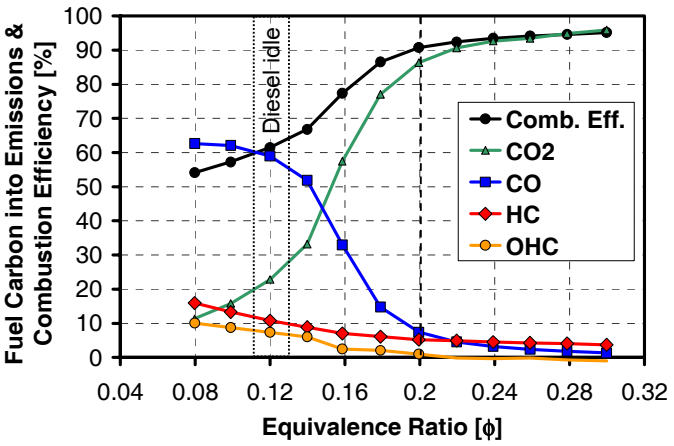

Figure 1. Exhaust emissions as function of fueling rate for fully pre-mixed fueling for iso-octane, CA50 = TDC, 1200 rpm, from Ref. [11].

octane and air, at a compression ratio (CR) of 18 (reproduced from Ref. [11]). The emissions are given as the percentage of total fuel carbon in each of the exhaust species to remove changes due solely to the quantity of fuel supplied. The 50% burn point (CA50) was held constant at top dead center (TDC). At intermediate loads, where ϕ is above 0.2 (right of the dashed line in Fig. 1), CO and HC levels are low, and carbon dioxide (CO_2) levels are high, resulting in high combustion efficiencies, on the order of 95%. As discussed in previous works [3,12-14], the small combustion inefficiencies at these higher loads are thought to result primarily from unburned or partially reacted fuel in the crevices or near-wall regions. However, when ϕ is decreased below 0.2 (to the left of the dashed line), CO levels start to rise rapidly, and HC and OHC also begin to increase, while CO_2 levels sharply decrease. As a result, combustion efficiency drops, reaching unacceptable levels of about 60% at diesel idling conditions ($0.11 \le \phi \le 0.13$). At these low loads, the mixtures are so dilute that combustion temperatures are too low for the bulk-gas reactions to go to completion before they are quenched by the expansion stroke [3-5,8,14,15]. Previous works have generally focused on the bulk-gas CO-to-CO_2 reactions becoming incomplete (causing the high CO emissions) as peak combustion temperatures are reduced below about 1500 K [3,5,8]. However, when temperatures become sufficiently low (*i.e.*, well below 1500 K), the first steps of fuel oxidation or even the fuel breakdown reactions become too slow to go to completion [3,8]. Thus, the in-cylinder locations where HC and OHC emissions form vary with fueling rate.

As discussed above, typical exhaust-gas analyzers are less sensitive to OHC compounds, so a direct measurement of total OHC emissions is not easily obtained. However, it was noted that closing the carbon balance between the exhaust species and the supplied fuel showed an increasing amount of carbon unaccounted for as ϕ was reduced below 0.2 [3]. The trend in the quantity of this "missing" carbon is generally the same as that expected for the amount of OHC emissions based on single-zone modeling results [3,8]. Therefore, this error in carbon-balance closure is shown as OHC emissions in Fig. 1, as discussed more completely in Ref. [3]. Clearly, this is not an accurate measurement of the total OHC since it includes the accumulated errors from all the measurements (CO, CO_2, and HC). For example, the data in Fig. 1 show non-physical, slightly negative OHC values for $0.22 \le \phi \le 0.3$, as a result of small errors in the other measurements. Nevertheless, this carbon-closure measurement gives an indication of the expected trends in OHC.

Because of the difficulty in measuring OHC species, their presence in HCCI exhaust was not noted until 2002, when they were reported independently in three separate studies [8-10] and later verified in a fourth study [16]. These previous studies also provided some information on the individual OHC and HC species, as follows:

- Dec [8] presented single-zone computational results showing that significant concentrations of OHC compounds should be present in HCCI exhaust at low loads, and that the amount of OHC should increase with reduced fueling, as bulk-gas combustion becomes less complete. In a subsequent paper, Dec and Sjöberg [3] identified the most prevalent of these species as formic acid, formaldehyde, acraldehyde, and acetaldehyde, based on computational results for iso-octane, using the detailed mechanism from LLNL [17]. They also noted that the computations predicted methane to be the most prevalent HC species from the bulk gas at low loads.
- Kaiser *et al.* [9] presented experimental exhaust speciation data from a gasoline-fueled HCCI engine obtained using gas-chromatography combined with a FID or a mass spectrometer (GC-FID and GC-MS). They identified three OHC species: formaldehyde, acetaldehyde and benzaldehyde, and showed that the percent of fuel carbon in these species increased as fueling was reduced. In a follow-on work, Kaiser *et al.* [18] presented emissions data in tabular form for a large number of HC and OHC species for gasoline-fueled HCCI. They also plotted the trends of a few species, showing that the percent of fuel carbon in these species increases with decreased fueling.
- Iida *et al.* [10] used Fourier transform infra-red (FTIR) analysis to perform a limited exhaust speciation analysis for an HCCI engine fueled with *n*-butane. They found significant quantities of the OHC species formaldehyde and acetaldehyde. They also identified four HC species, with the most prevalent being unreacted fuel (*n*-butane), followed by ethene, methane, and propene. They also show a general trend of the concentration of all species increasing with reduced fueling.
- Later, Lemel *et al.* [16] also presented data confirming the presence of formaldehyde using FTIR analysis. In agreement with the other studies, they showed that its concentration increased with reduced fueling. This study also investigated the effect of fuel type, showing that formaldehyde concentrations were higher for two-stage-ignition fuels.

These previous investigations have added considerably to our understanding of HC and OHC emissions; however, there are many aspects that are still not well understood.

The objective of the current work is to obtain high-quality HC and OHC exhaust speciation data over a range of operating conditions, and to analyze these data to better understand the in-cylinder processes and sources of these emissions. To accomplish this, accurate HC and OHC species sampling and analysis techniques were developed. Then, using these techniques, data were acquired for two parametric sweeps in an HCCI engine. First, for premixed fueling, the fueling rate was varied incrementally from a mid-range load down to below-idle conditions. Second, since fuel/air mixture stratification can greatly improve low-load combustion efficiency [3,6,7], a gasoline-type direct injector (GDI) was used to systematically delay the start of injection (SOI) to vary the mixture formation from well-mixed to highly stratified conditions at an idle fueling rate of $\phi = 0.12$. The fuel selected for these studies was iso-octane, which is a good surrogate for gasoline in terms of engine operation [4]. However, unlike gasoline, this single-component fuel allows the species resulting from fuel breakdown to be easily understood and tracked. As fueling rate and mixture stratification are varied, the data show distinctly different trends for the various HC and OHC species. Analyzing these trends in terms of the expected progress of fuel breakdown and oxidation provides an improved understanding of the in-cylinder processes of HCCI combustion and emissions formation for both well-mixed and mixture-stratified operation.

In addition, using iso-octane as the fuel provides a database for comparison with single-zone, multi-zone, and full CFD models that use iso-octane chemical-kinetic mechanisms, as demonstrated in a concurrent paper [19]. Finally, this database of HC and OHC emissions will be helpful for the development of oxidation catalysts with appropriate low-temperature light-off characteristics, which will likely be needed to control these emissions from HCCI engines.

A description of the HCCI research engine facility and conventional data acquisition methods are given in the next section. This is followed by a description of the sampling and analysis techniques used for the detailed speciation of the HC and OHC emissions. Then, the results are presented in two parts corresponding to the equivalence-ratio and fuel-stratification sweeps. In the final section, the findings are summarized and conclusions are drawn.

EXPERIMENTAL SETUP

ENGINE FACILITY

The HCCI research engine used for this study was derived from a Cummins B-series medium-duty, six-cylinder diesel engine, which is a typical medium-duty diesel engine with a displacement of 0.98 liters/cylinder. Figure 2a shows a schematic of the engine, which has been converted for single-cylinder operation. The engine specifications and operating conditions are listed in Table 1. A complete description of the engine and facility may be found in Ref. [3].

The engine was equipped with a custom HCCI piston as shown in Fig. 2b. This combustion chamber design was chosen because it provided a large squish clearance and a minimum top ring-land crevice volume that amounts to only 2.1% of the top dead center (TDC) volume (including the volume behind the top piston ring) for the 14:1 compression-ratio piston used in this study.[1] Most of our previous low-load HCCI studies with iso-octane and gasoline fueling, including the data presented in Fig. 1, used a CR = 18 piston with naturally aspirated intake conditions [3-5,11]. However, a CR = 14 piston was installed in the engine for other concurrent studies, so we maintained this CR = 14 for the current investigation. With CR = 14 and an intake pressure (P_{in}) of 100 kPa, the intake heating system (which was limited to approximately 230°C) was not sufficient for low-load combustion of iso-octane. Therefore, the intake pressure was boosted to 135 kPa, so the TDC pressure with CR = 14 matched that with CR = 18 and P_{in} = 100 kPa. The intake temperature (T_{in}) was also increased to match the TDC temperature of the CR = 18 cases, and was adjusted as necessary to maintain the 50% burn point at TDC. This required $180°C \le T_{in} \le 210°C$ for intake equivalence ratios from 0.28 to 0.08, respectively. With these adjustments, the combustion efficiency, CO, and HC levels for the CR = 14 data were nearly identical to the older CR = 18 data, as shown in Ref. [7].[2] There were small differences in the CO_2 levels, mainly as the result of a new CO_2 analyzer. This difference also produced a difference in the estimated OHC values deduced from the carbon closure, as will be shown later. The effects of fuel stratification on overall emissions and combustion efficiency were also quite similar for the two compression ratios [7].

The engine was equipped with two fueling systems. For the equivalence-ratio sweep, fueling was accomplished with a fully pre-mixed fueling system using an electrically heated fuel vaporizer, as shown near the top of Fig. 2a. For the investigation of mixture-stratified operation, fuel was supplied by an 8-hole GDI injector mounted in the center of the cylinder head. The sprays from this injector had a 70° included angle (Fig. 2c). In order to accurately determine the amount of fuel supplied, a positive-displacement flow meter was installed on the common fuel line that supplies either the injector in the engine or the injector in the vaporizer. The meter was calibrated by mass at multiple flow rates, using the same fuel-supply system used for engine operation. All injection timings given are the actual start of injection. The injec-

[1] It should be noted that the valve pocket and head gasket crevices, which are not shown in Fig. 2b, contribute to the TDC volume, making the actual CR = 14.

[2] Although the differences in intake conditions and CR cause the pressure and temperature histories to be different for the two data sets, the differences are very small near TDC, and thus appear to have little effect on these data for which CA50 = TDC, and the 10-90% burn duration is only 3.5 – 11°CA.

TABLE 1. Engine Specifications and Operating Conditions

Displacement (single-cylinder)	0.981 liters
Bore	102 mm
Stroke	120 mm
Connecting Rod Length	192 mm
Geometric Compression Ratio	14:1
No. of Valves	4
IVO	0°CA*
IVC	202°CA*
EVO	482°CA*
EVC	8°CA*
Swirl Ratio	0.9
Injector Type	8-hole, GDI
Injector Spray (included angle)	70°
Injection Pressure	120 bar
Engine Speed	1200 rpm
Intake Pressure	135 kPa (abs.)
Coolant Temperature	100°C
Fuel	Iso-Octane

* 0°CA is taken to be TDC intake. The same camshaft is used as in previous studies, but the valve-event timings have been slightly adjusted to better represent the point of 0.1 mm lift.

tion duration was 0.63 ms (4.5°CA) at the fueling rate used for the SOI sweep ($\phi = 0.12$).

The intake air was supplied by an air compressor and electrically heated to the desired intake temperature. An auxiliary heater located close to the engine (see Fig. 2a) precisely controlled the intake temperature so the combustion phasing could be maintained with 0.2° crank angle (CA) of the desired value. The air flow was metered and controlled by a sonic-nozzle orifice.

Prior to running, the engine was preheated to 100°C by electrical heaters on the "cooling" water and lubricating oil circulation systems, and this temperature was held steady during the experiments. At each operating point, the engine was allowed to run for several minutes until all measured parameters were stable, at which point the data were acquired.

Iso-octane was the fuel used for this study, as discussed in the Introduction. All data were taken at an engine speed of 1200 rpm, with the intake air flow adjusted to maintain P_{in} = 135 kPa (absolute). No exhaust-gas recirculation was used.

CONVENTIONAL DATA ACQUISITION

Cylinder pressure measurements were made with a piezoelectric transducer (AVL QC33C) at ¼°CA increments. The measurements were pegged (adjusted to match) to the intake pressure near bottom dead center (BDC) where the cylinder pressure reading was virtually constant for several degrees. For all data presented, 0°CA is defined as TDC at the start of the intake stroke (so TDC compression is at 360°). This eliminates the need to use negative crank angles or combined BTDC, ATDC notation.

For all experiments, the combustion phasing was controlled so that the 50% burn point (CA50) was maintained

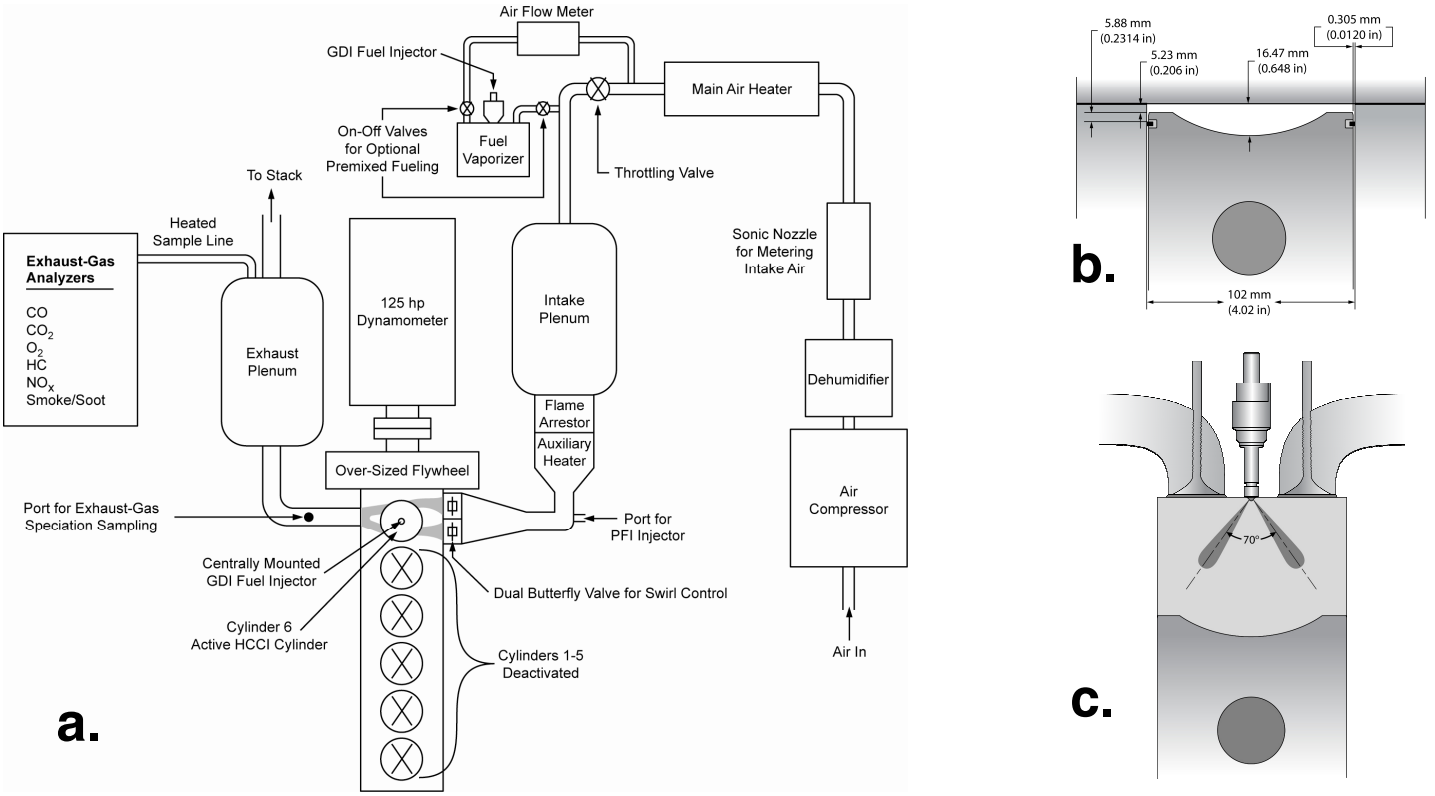

Figure 2. Schematics showing: a) the HCCI engine facility, b) combustion chamber dimensions at TDC, and c) the layout and spray angle of the 8-hole GDI fuel injector, with the piston at the 280°CA position.

at TDC (360°CA). CA50 was determined from the cumulative apparent heat-release rate (AHRR), computed from the cylinder-pressure data (after applying a 2.5 kHz low-pass filter [3]). Computations were performed for each individual cycle, disregarding heat-transfer and assuming a constant ratio of specific heats [20]. The average of 100 consecutive individual-cycle CA50 values was then set to TDC by adjusting the intake temperature.

Conventional exhaust emissions data were also acquired, with the sample being drawn from the exhaust plenum using a heated sample line (see Fig. 2a). CO, CO_2, HC, NO_X, and O_2 levels were measured using standard exhaust-gas analysis equipment as listed in Table 2. Smoke measurements were made with an automated smoke meter, but levels were zero or near-zero for all conditions studied and are not reported.

Table 2. Emissions-Bench Analysis Equipment

CO	Non-Dispersive Infrared Detector, Rosemount 880A
CO_2	Non-Dispersive Infrared Detector, California Analytical Instruments 602
HC	Flame Ionization Detector (FID), Rosemount 400A
NO_X	Chemiluminescence Analyzer, Rosemount 951A
O_2	Paramagnetic Analyzer, Rosemount 755R
Smoke	Optical-Density of Filter Paper, AVL415S

DETAILED HC AND OHC SPECIATION SAMPLING AND ANALYSIS

SAMPLING

Exhaust samples for detailed speciation were collected in Tedlar gas sampling bags. Bags were prepared by three successive evacuations and purgings with dry nitrogen. A separate sample was collected for formaldehyde and acetaldehyde using a dinitrophenylhydrazine (DNPH) derivatizing solution as described by Lipari and Swarin [21]. The solution was prepared by dissolving 500 mg reagent grade DNPH in 2-normal hydrochloric acid under a dry nitrogen atmosphere. A new batch of DNPH solution was prepared before each experiment.

All samples were drawn from a small port on the exhaust runner located between the cylinder head and the exhaust plenum (Fig. 2a). Fitted to the port was a valve that provided the option to direct flow into two different 1/8 inch Teflon tube sampling lines wrapped in heating tape. One line led to a small pump that filled a 500 ml or one-liter Tedlar bag at 2 liters per minute. Two separate bag samples were collected, one for the C1-C2 hydrocarbons, and the other bag for the remaining species. The other line was attached to two 25 ml Pyrex sparge tube vessels connected in series with Teflon fittings. The vessels were filled with DNPH solution. Exhaust was pulled through the DNPH solution at 100 cubic centimeters per minute using a small pump whose rate was controlled by a small needle valve upstream of the sparge tubes. Optimal flow rates were determined in the lab by pulling formaldehyde and acetaldehyde standards from a Tedlar bag. Collection efficiency of these standards was ~100%, measured by the recovery of the derivatized aldehydes. During exhaust sample collection, average flow rates and collection times were recorded using an electronic flow meter. Sampling times ranged from 3 – 20 minutes depending on anticipated concentrations. Excessive sample times resulted in a light precipitate forming in the DNPH solution. The DNPH solution was maintained at room temperature during sampling. Immediately after sampling it was transferred to an amber-colored glass bottle and sealed with a Teflon-lined cap.

ANALYSIS

The C1-C2 hydrocarbons were analyzed using an SRI 8610C gas chromatograph equipped with a flame ionization detector. Samples were introduced using an electronically actuated VICI/Valco multiport gas sampling valve with a 1.0 ml sample loop, with direct injection into a 6 ft x 1/8 inch stainless steel silica gel packed column, using helium as the carrier gas. Fixed gas standards were purchased from Supelco and used for calibration.

All other hydrocarbons and oxygenated hydrocarbons were analyzed using an HP5890/5972MSD gas chromatograph mass spectrometer (GC-MS) within one week of collection. A Tedlar bag sample and a 25 ml gas-tight syringe were first heated in an oven to 60°C. A 25 ml aliquot was drawn into the syringe and subsequently injected directly into a heated glass tube purged with a 25 cc/min high-purity helium flow. The helium swept the sample onto an adsorbent comprised of a mixture of Carbopak B and carboxen (Supelco VOCARB 3000). After 20 minutes the trap was heated to 250°C and the adsorbed species were concentrated onto the head of the GC column using the helium flow. Compound separation was facilitated using a DB-502 capillary column heated from 35°C to 250°C at 5°C/min and held for 10 minutes. Injector and detector temperatures were held at 225°C and 250°C, respectively. Standards were prepared by injecting 1-5 microliters of authentic standards into a Tedlar bag filled with dry nitrogen and analyzed using the same method.

For quantitative analysis, the standard preparations were injected at three different concentrations and total ion currents (TICs) were integrated for linear regression analysis. For most species detected and identified in the exhaust samples, the TICs were sufficient for producing concentrations that were consistent with anticipated levels implicit in the standard exhaust-gas analysis equipment. However, some species required quantification using specific ion fragments, since several showed significant overlap with a broad water peak or a co-eluting species. Eleven different authentic standards were used in total, some of which were the same as those detected in exhaust samples, but others were chosen for their similarity to a large number of exhaust species in order to simplify the quantitative analysis. With the exception of formaldehyde, response factors varied by approximately a factor of two among hydrocarbon standards, and a factor of seven for oxygenated hydrocarbons. Standards with similar structures to exhaust species

were routinely matched for quantification when an authentic (*i.e.* exactly matching) standard was not available.

DNPH samples were processed in duplicate by aliquoting 200 microliters of solution into a 10 ml vial and adding 2 ml of hexane (95% n-hexane purity). The vial was sealed and shaken for one minute and the immiscible phases were allowed to separate. Then the hexane layer was pippetted into a glass centrifuge tube and dried at <50°C under a gentle stream of dry nitrogen. The dried residue was re-dissolved in acetonitrile. Authentic formaldehyde and acetaldehyde standards were also derivatized and extracted to determine the method recovery efficiencies, which were 55±5% and 77±5% for formaldehyde and acetaldehyde, respectively. For low concentrations, the sample was extracted a second time with hexane, and recovery efficiency was >80%. Results from routine duplicate extractions were typically in agreement to ≤10%. After extraction, samples were measured for derivatized products using a ThermoFinnigan Survey high-performance liquid chromatograph (HPLC). Compound separation was facilitated by a C18 stationary phase and gradient elution starting with a 5% acetonitrile/95% water mobile phase and ending with 20% acetonitrile/80% water over 24 minutes of analysis time. Multiple wavelength photodiode array detection of compounds was initially used to identify formaldehyde and acetaldehyde derivatives, but a wavelength of 360 nm was routinely used in calibration.

Comparison of the GC-MS and DNPH HPLC methods is useful for understanding analytical errors over various concentration levels. For example, the formaldehyde results suggest that the two methods produce similar results to within 20% of each other (Table 3). However, the results using the DNPH HPLC method are considered here as more representative of actual concentrations because we had better experimental controls, better agreement with measurements using the standard emissions-bench exhaust-gas analysis equipment, and smoother trends over the two parametric sweeps. Consequently, GC-MS appears to over-represent the concentration at lower levels, whereas it under-represents at high levels. The latter is likely due to losses during sample storage and introduction into the instrument before analysis, whereas the former reflects limits to preparation and analysis of low concentration standards. The HPLC values are used for all of the data presented in the Results section.

Table 3. Comparison of formaldehyde results between GC/MS and DNPH HPLC methods for the ϕ-sweep experiment.

ϕ	ppm CH_2O (GC-MS)	ppm CH_2O (DNPH HPLC)	Difference
0.28	17.6	14.8	2.8
0.24	26.9	15.7	11.2
0.20	25.1	20.9	4.2
0.16	40.3	46.1	-5.8
0.12	72.7	92.4	-19.7
0.08	109.2	125.2	-14.0

RESULTS AND DISCUSSION

EQUIVALENCE-RATIO SWEEP

As discussed in the Experimental section, the engine was configured with a CR = 14 piston, with P_{in} and T_{in} increased to match the TDC conditions of previous studies with CR = 18. Figure 3 shows a plot of the normalized emissions as a function of ϕ. These data were acquired using the conventional emissions-bench analyzers, simultaneously with the detailed speciation measurements. As can be seen, the curves are nearly identical to those in Fig. 1 for CR=18, indicating that the approach of matching TDC conditions results in very similar combustion. The only noticeable difference is that the OHC curve, which is based on the carbon-balance closure (discussed in the Introduction), is flatter. This is mainly due to differences in the CO_2 readings, resulting from a new CO_2 meter, as discussed previously.

Comparison of Total Detailed-Speciation HC and OHC with Emissions-Bench Data – Before presenting the detailed-speciation results, it is useful to compare the total HC and OHC emissions from the detailed-speciation measurements with the emissions-bench data as a cross check on the two data acquisition systems. For this comparison, the detailed speciation data were adjusted to match the expected response of the FID-based analyzer used to obtain the HC emissions-bench data. Accordingly, the total HC from the detailed-speciation measurements includes not only the sum of all the carbon from the HC species, but also the sum of the carbon atoms from the OHC species that are not attached directly to oxygen atoms. Similarly, the total OHC from the detailed-speciation data includes only the carbon atoms that are directly attached to oxygen atoms. (For example, acetone, which contains three carbons and one oxygen, will count as two HC carbon atoms and one OHC carbon atom). This comparison is shown in Fig. 4. Note that the emissions-bench HC and OHC data are the same as those in Fig. 3.

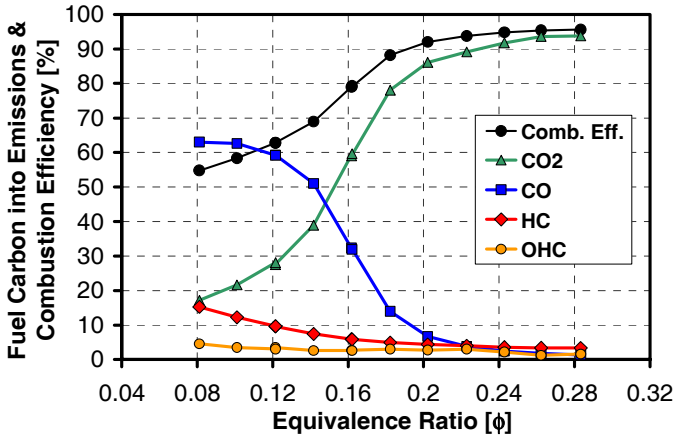

Figure 3. Conventional emissions-bench measurements of global emissions shown as percentage of total fuel carbon. NO_X emissions were near zero and are not reported. CR = 14; P_{in} = 135 kPa; T_{in} was adjusted to obtain CA50 = TDC at each ϕ.

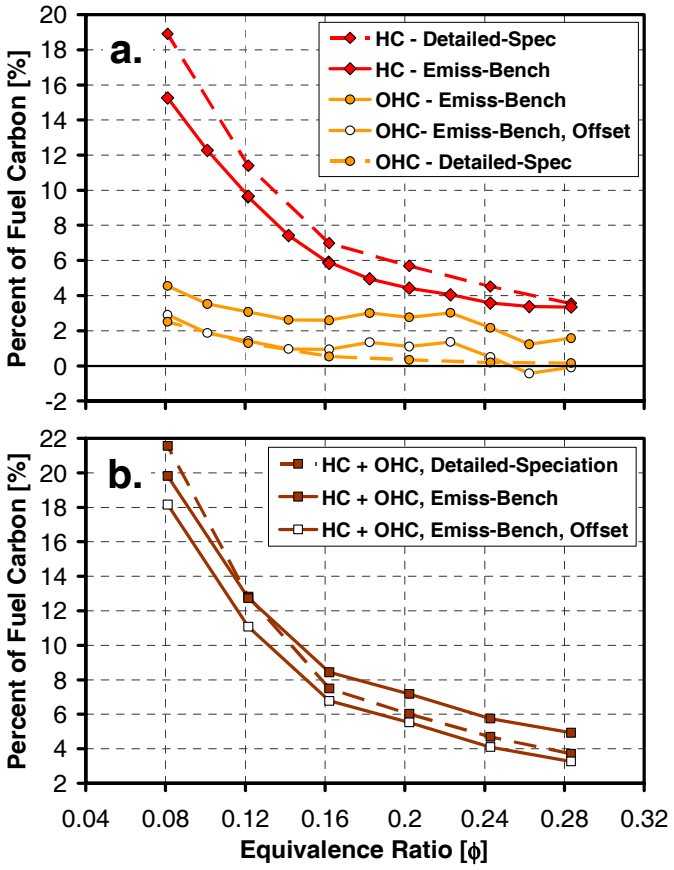

Figure 4. a) Comparisons of total HC and OHC for conventional emissions-bench measurements (solid lines) and the sum of the detailed-speciation measurements (dashed lines). b) Comparison for the sum of the HC and OHC species.

As evident in Fig. 4a, the comparison between the HC values for the two techniques is very good. It varies from almost an exact match at ϕ = 0.28 to about a 20% discrepancy at ϕ = 0.08, with the sum of the detailed speciation measurements consistently showing slightly higher values. In contrast, the OHC curves show significant differences. The total OHC from the detailed-speciation measurements is near zero at the higher loads ($0.2 \le \phi \le 0.28$) and shows a continuous, smooth trend of increasing toward lower loads for $\phi < 0.2$. This is consistent with what is expected from increasingly incomplete bulk-gas combustion as shown by the single-zone model in Ref. [3] and with our previous emissions-bench OHC values as shown in Fig. 1. In contrast, the current emission-bench OHC shows an offset of about 1.5% fuel carbon, and the trends are somewhat erratic. As discussed above, there is substantial uncertainty in this curve since it is based on the carbon-balance closure, causing it to be affected by small errors in the other exhaust analysis instruments. Assuming that this is the case, the curve has been offset to bring the average of the three highest ϕ values in-line with those of the detailed speciation curve. As can be seen, with this offset the general trend of the emissions-bench curve matches that of the detailed-speciation OHC curve. Since this general trend matches, and because considerable care was taken in obtaining accurate OHC concentrations in the detailed analysis, we believe that the detailed-speciation curve is correct.

Since there is some uncertainty to the response of the emissions-bench FID to the oxygen-bound carbon, the total HC + OHC carbon is also compared in Fig. 4b. As can be seen, the measurements are in generally good agreement, with the adjusted emissions-bench data (offset OHC data) giving a better match at higher loads. Based on these comparisons, the detailed speciation data are considered to be sufficiently accurate, and only the detailed speciation data will be presented for the remainder of this section.

Detailed Speciation Data – Figure 5 shows the most prevalent HC and OHC emissions species and their trends with fueling rate (ϕ). Also shown are the total HC and OHC emissions to provide a basis for estimating the contribution of each emissions species to the total. To facilitate this comparison, the total HC and OHC emissions are not adjusted to match the emission-bench FID response as they were in Fig. 4a. Rather, the HC curve shows the total percentage of fuel carbon in all the HC species, but not any fuel carbon from the OHC species. Similarly, the OHC curve shows all the fuel carbon in the OHC species, both the carbon atoms that are attached to an oxygen and those that are not. To help distinguish HC and OHC species, they are shown with diamond and circle symbols, respectively, in Fig. 5 and in all following figures. Also, to facilitate distinguishing the curves for the various species when printing in black and white, the order of the species in the legend corresponds to the order of the species in the plot at ϕ = 0.08, for Figs. 5 – 8.

As can be seen, by far the most prevalent emission is unreacted fuel, iso-octane. This is followed by 2-methyl-1-propene, which is a known breakdown product of iso-octane [18]. Following this, methane and the OHC species formaldehyde, acetone, and 2-methyl-2-propenal occur in almost equal quantities. As ϕ is decreased, the percent of fuel carbon in all the HC and OHC species increases, but iso-octane remains the largest contributor to the emissions. However iso-octane's contribution to the total HC+OHC decreases from 71% at the highest load (ϕ = 0.28) to only 36% at the lowest load (ϕ = 0.08). In contrast, 2-methyl-1-propene is in very low concentration at the high loads, contributing only 8% of the total HC+OHC, but its contribution increases to 14% of the total at the lowest load. Similarly, the other four species presented also show a large increase in their contributions to the total as the fuel load is decreased. Thus, the increase in HC and OHC emissions with reduced fueling is driven mainly by an increase in the contributions of species with a smaller molecular size than iso-octane. Finally, it is interesting to note that unlike the HC emissions, no one species dominates the OHC emissions, with formaldehyde, acetone, and 2-methyl-2-propenal each making up about 20% of the total OHC at the lowest load (the remainder belonging to lower-concentration species as shown below).

Several other HC and OHC species occur in lesser quantities. The most significant of these are plotted with an expanded scale in Fig. 6 along with the lower-concentration species from Fig. 5. A complete list of all species detected and their concentrations is given in tabular form in the Appendix. In Fig. 6, the HC and OHC compounds are shown on separate graphs, Figs. 6a and 6b, respectively, to prevent the plots from becoming too cluttered with overlapping curves. As with the more-abundant species, the percentage of fuel carbon in all the lesser species increases with decreasing fueling. However, the relative abundance of the various species and their rates of increase with reduced fueling vary significantly.

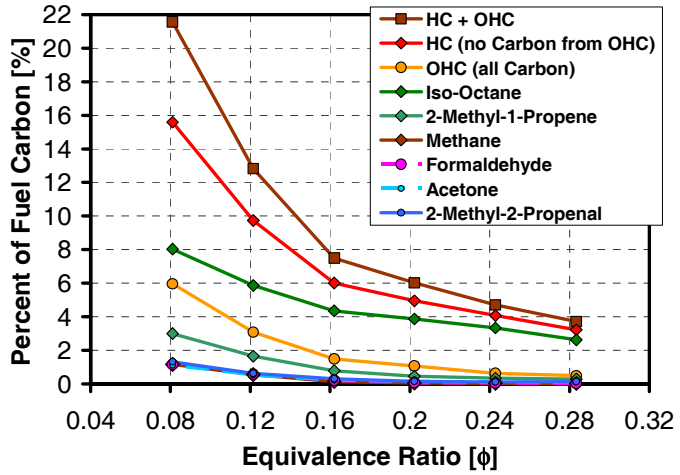

Figure 5. Main HC (diamonds) and OHC (circles) species. Note the that last four species listed are essentially overlapping. The total HC + OHC curve is the same as in Fig. 4b, but the HC and OHC curves are not adjusted to match FID data, but rather show the total of all the carbon in the HC and OHC species, respectively.

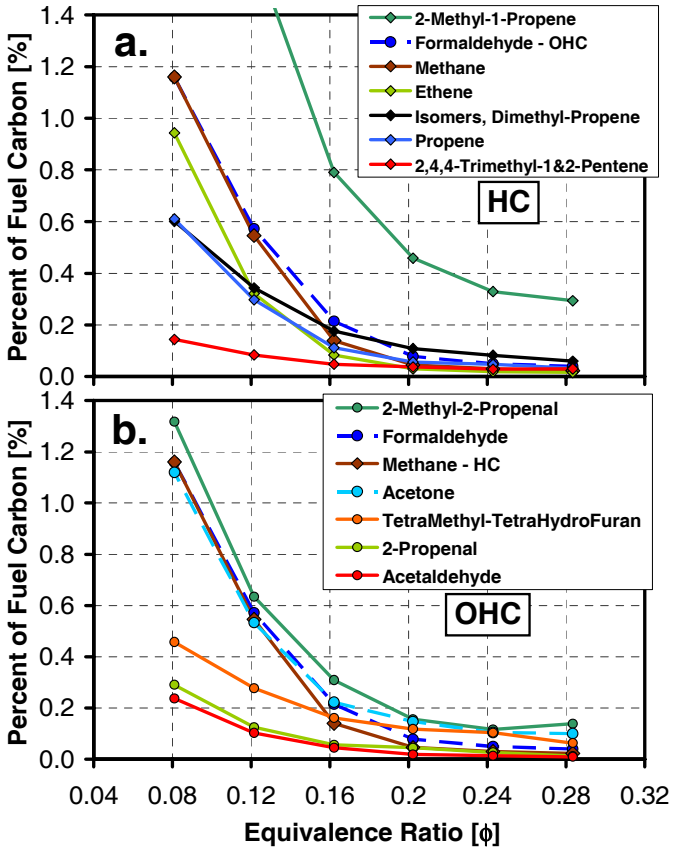

Figure 6. Lesser HC (a) and OHC (b) species. To assist comparison between the plots, the OHC species, formaldehyde, is shown on the HC plot and the HC species, methane, is shown on the OHC plot.

Examining the HC and OHC species in Figs. 5 and 6 shows that these emissions can be broadly separated into three categories: 1) the parent fuel, iso-octane, and species that are closely related in molecular structure to the parent fuel, 2) species that have one or more carbon atoms less than iso-octane, but still show some related molecular structure, and 3) small molecules that have no direct resemblance to the parent molecule and could have resulted from the breakdown reactions of almost any hydrocarbon fuel.

Figure 7 shows the molecular structure of the HC and OHC species in the first two categories. In the left-hand column are molecules belonging to the first category. At the top is the parent fuel molecule 2,2,4-trimethyl-pentane (iso-octane). Next is 2,4,4-trimethyl-1-pentene, which is the same as the parent fuel except that two hydrogens have been abstracted and replaced with a double bond. The double bond can also occur in the second position and in Fig. 6a, the sum of 2,4,4-trimethyl-1-pentene and 2,4,4-trimethyl-2-pentene is plotted. The last molecule in this category is tetramethyl-tetrahydrofuran. As can be seen from the drawing, this

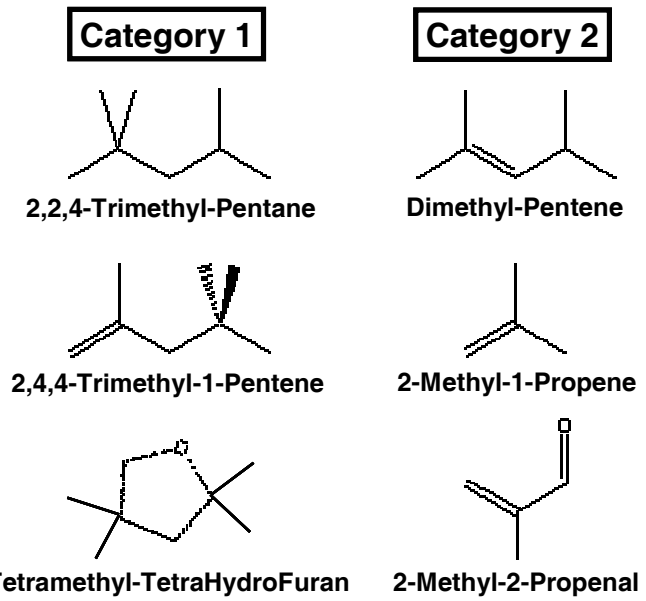

Figure 7. Molecular structures of the larger HC and OHC emissions. Left column shows the fuel, 2,2,4-trimethyl-pentane (iso-octane), and molecules that have only hydrogen abstraction and oxygen addition. The right column show further breakdown species with one or more carbons missing.

molecule is formed from the parent fuel when two hydrogens are abstracted and an oxygen atom is bound between the two removed-hydrogen sites.

The right-hand column of Fig. 7 shows molecules belonging to the second category. Dimethyl-pentene is formed when one methyl group and one hydrogen are removed from 2,2,4-trimethyl-pentane and replaced with a double bond. Three different isomers of dimethyl-pentene (4,4-dimethyl-2-pentene, 2,4-dimethyl-1-pentene, and 2,4-dimethyl-2-pentene) were identified in the emissions and their sum is plotted in Fig. 6a. Next is 2-methyl-1-propene. As mentioned above, this molecule has been shown to be a prevalent breakdown product of iso-octane [18], and examination of its structure indicates that it could be formed by breaking dimethyl-pentene in half, or by breaking a four-carbon group off of trimethyl-pentane or trimethyl-pentene. The final molecule in this category is 2-methyl-2-propenal, which is nearly the same as 2-methyl-1-propene except that an oxygen is attached. This molecule (also known as methacrolein) has also been shown to be a breakdown product of iso-octane [18].

In the third category are smaller species with one to three carbon atoms, whose molecular structure cannot be directly linked to the parent fuel. The three-carbon species are propene, 2-propenal and acetone; the two-carbon species are ethene and acetaldehyde; and the one-carbon species are methane and formaldehyde. In addition to the species shown in Figs. 5 and 6 and discussed above, several other species were identified. However, their concentrations were quite low, and they will not be further discussed.

Spatial Location of HC and OHC Species Formation – In presenting the various HC and OHC emission species above it was noted that although the percent of fuel carbon in all species increases with reduced ϕ, the rate of increase varies significantly between species. For example, as shown in Fig. 6a, some species, such as trimethyl-1&2-pentene, show only a small increase while others, such as methane and formaldehyde, show a large increase (see Fig. 6a). More careful examination shows that in general, species in category 1 tend to have a smaller increase with reduced ϕ than those in category 2, while those in category 3 have the largest increase. However, this can be difficult to see in Figs. 5 and 6 because the emissions level (percent of fuel carbon) differs greatly between the various species. Also, the values of most of the species are quite low at the higher ϕ values, and the curves overlap.

To better visualize differences in the trends with ϕ, the data in Figs. 5 and 6 are replotted in Fig. 8 with their values normalized by their respective ϕ = 0.28 values. Thus, these curves show the factor by which the percent fuel carbon of each species increases over its value at the highest load (the "increase factor"). The differences in the trends of the various emission species are now clear.

Moreover, the curves are now ordered in terms of the amount of fuel breakdown and reaction towards full combustion. As can be seen, the species having the least change with ϕ is the unreacted fuel, 2,2,4-trimethyl-pentane, which increases by a factor of 3 as fueling is reduced from ϕ = 0.28 to ϕ = 0.08. Next is 2,4,4-trimethyl-1&2-pentene, the species that represents the

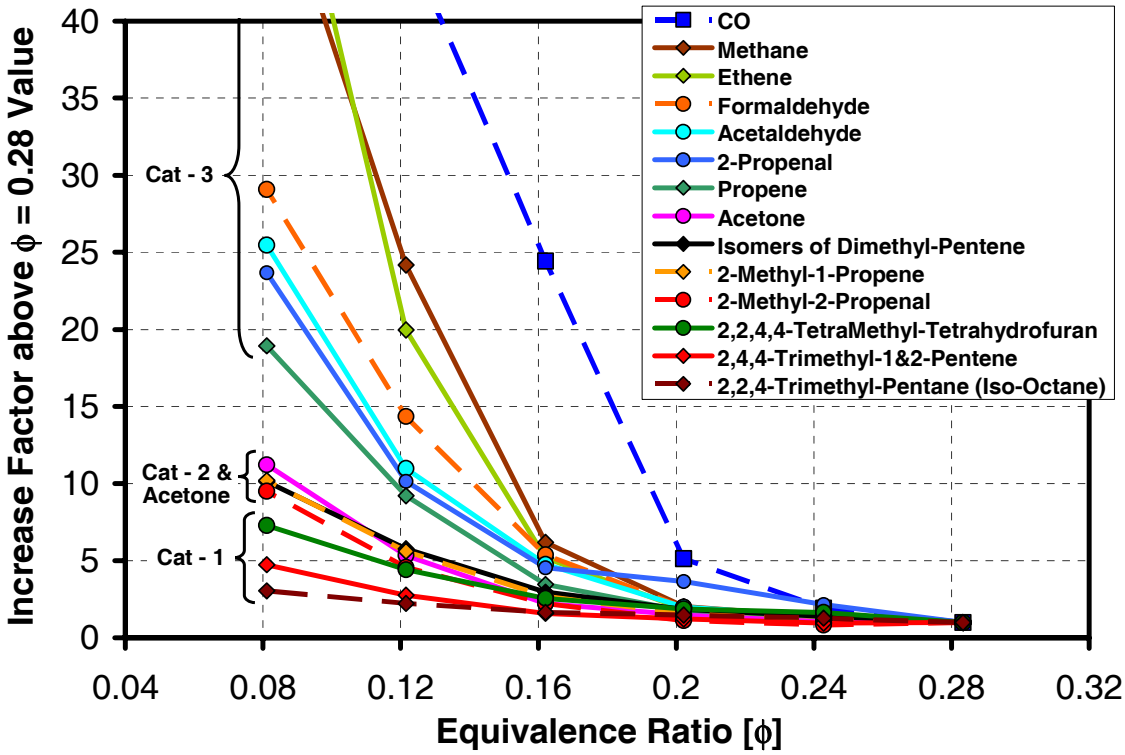

Figure 8. Normalized emissions of HC, OHC, and CO as a function of ϕ. For each curve, the percentage of fuel carbon has been normalized by its value at ϕ = 0.28, thus providing the "increase factor" above the ϕ = 0.28 value.

smallest change from the parent fuel molecule, as discussed above. Following this is the third category-1 species tetramethyl-tetrahydrofuran. Above these are the curves for the category-2 species. Interestingly, the curves for all three of these compounds (isomers of dimethyl-pentene, 2-methyl-1-propene, and 2-methyl-2-propenal) nearly overlap. Next are the category-3 species. The acetone curve nearly overlaps those of the category-2 species, and this is followed by the other three-carbon species (propene and 2-propenal). The smallest category-3 species show the largest relative increase as ϕ is reduced, with the increase factors of ethene and methane approaching that of CO.

Overall these normalized data show a very strong trend of a greater proportional increase with reduced ϕ as fuel breakdown progresses. One exception is that for the category-2 species and acetone, the normalized curves nearly overlap, rather than showing clear trends with molecule size. This might be the result of small inaccuracies in the data. Since these curves are normalized by their respective ϕ = 0.28 values, for which the absolute concentration is quite low, a strong demand is placed on the accuracy of the measurement of a small quantity. As discussed previously, care was taken to insure good accuracy, but small errors could have affected these curves somewhat. However, it is also entirely possible that the observed trends are real, and occur because all these species form in the same temperature range as discussed below. One explanation for this is that breakdown reactions of the larger category-1 molecules cause them to "split" in such a way that they form two category-2 species (*e.g.* two 2-methyl-1-propene molecules), or a category-2 species and a smaller species like acetone.

The strong trends with the steps of fuel breakdown in the normalized emissions data in Fig. 8 can be related to regions within the cylinder where these emissions are expected to form. To facilitate this explanation, it is helpful to refer to the expected average in-cylinder temperature distribution. Figure 9 reproduces the in-cylinder temperature distribution at TDC for motored operation computed using KIVA by Aceves *et al.* [14] for a previous study in this engine. Operating conditions were similar to the current study, except that the compression ratio was 18:1, so the scallop (shallow bowl) in the piston was not as deep, and the intake pressure was 120 kPa. These differences should not affect the general trends, which is all that will be discussed here. Accordingly, the motored TDC temperature distribution in Fig. 9 can be considered representative of the temperature distribution at the start of combustion in the current study.

As can be seen, the top ring-land crevice region is quite cold, and there is a temperature gradient from the wall outward through the boundary layer to the bulk gas, which is at the highest temperature. It can also be seen that the gradient is quite steep near the wall and at the entrance to the ring-land crevice. Moving away from the wall, the temperature gradient becomes progressively less steep, and is quite shallow as the boundary layer merges into the bulk-gas. To first order, combustion will

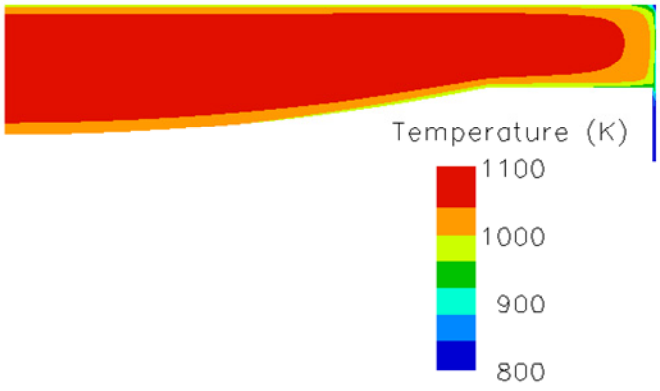

Figure 9. Motored-engine temperature distribution at TDC from KIVA modeling. Reproduced from Aceves *et al.* [14]. Shown is a slice from the centerline (left) to the cylinder wall (right). Note the top ring-land crevice at the lower right.

raise the temperature above this initial distribution, by an amount proportional to the combustion heat release at each ϕ. As ϕ is progressively reduced, the reduced combustion heat release will cause increasingly greater regions of the charge mass to fall below the temperature of complete combustion due to the shape of the boundary-layer temperature gradient. This effect explains the progressive change in the HC and OHC emissions with reduced ϕ, as discussed in the following paragraphs.

At the highest load (ϕ = 0.28), the combustion heat release is sufficient to raise the combustion temperatures above 1500 K and complete the reactions [5] throughout the bulk gas and the vast majority of the boundary layer. However, the ring-land crevice is so cold that virtually no reactions occur, making it a source of unreacted fuel. Fuel would also escape reaction in the head-gasket crevice, which is not shown, but would be located in the upper right corner of the distribution image in Fig. 9. Therefore, for the ϕ = 0.28 case, the temperature zones where intermediate HC and OHC species and CO are produced are only a series of thin layers between the unreacted fuel in the crevices and the complete-combustion regions in the bulk-gas and boundary layer, and/or a thin layer or layers next to the wall [14]. Thus, there are significant emissions of iso-octane at high loads, but only very low levels of all the other species (Figs. 5 and 6).

As ϕ is reduced, the combustion heat release is less, and the peak temperatures of all the regions are reduced. However, for $0.2 \leq \phi \leq 0.28$, the combustion heat release remains sufficiently high that the combustion still goes to completion over almost all of the charge volume, and the emissions levels increase only slightly. This is because the temperature gradient is very steep near the wall and fairly steep at the entrance to the crevices. Therefore, as the combustion heat release is first reduced from the highest load, only a small fraction of the charge mass, very near the wall and at the entrance to the crevices, falls to temperatures where combustion is incomplete. As a result, emissions of all species rise only slightly.

However, further reductions in ϕ have a much larger impact on the emissions. This is because the temperature gradient becomes progressively less steep farther from the walls (see Fig. 9), so the reduced combustion heat release brings increasingly greater portions of the charge mass below the temperature required for complete combustion. The first species that should be affected is CO, which is the closest intermediate to complete combustion, and which is not converted completely to CO_2 when local temperatures fall below about 1500 K [5]. In agreement, Fig. 8 shows the onset of the rise in CO occurring at the highest ϕ of any of the emission species. The next species to be affected are the smallest (category-3) HC and OHC molecules, which represent the farthest departure from the parent fuel, and therefore, presumably require a higher temperature to form than the other HC and OHC emissions. However, their formation temperature is still lower than that required for substantial conversion to CO, and in agreement, the onset of the rise of these species occurs at a lower ϕ than that of CO (see Fig. 8). This trend continues into the category-2, and then, the category-1 species, which are formed at successively lower temperatures. Also, for each individual species, the amount of emissions increases with reduced ϕ because its formation-temperature zone moves progressively farther out through the boundary layer. Therefore, a larger portion of the charge mass exists at this formation temperature due to the shallower temperature gradient farther from the wall. With a sufficient reduction in ϕ, eventually the emission species can arise from the entire bulk-gas. This occurs for CO at the lowest equivalence ratios of this study, causing CO levels to reach a maximum as shown in Fig. 3. However, none of the intermediate HC or OHC compounds reach this point for the ϕ range investigated.

In contrast with the smaller species, unreacted fuel shows only a modest increase with reduced ϕ. This is because its source is dominated by the crevice volume. With reduced ϕ, regions too cold for any reaction of the parent fuel increase, but they do not extend far into the boundary layer even at the lowest ϕ. Similarly, trimethyl-1&2-pentene increases only slightly, but it increases more than the fuel since its formation requires slightly higher temperatures, which occur a little farther out in the boundary layer. This trend continues with tetramethyltetrahydrofuran and the other HC and OHC species that show progressively greater reaction from the parent fuel molecule, and therefore, require progressively higher temperatures for formation.

This preceding explanation can be briefly summarized by saying that the trends in the detailed-speciation data indicate that the unreacted fuel and larger HC/OHC emissions arise from the crevices and near-wall regions, while the lighter HC/OHC emissions arise from the outer boundary layer and eventually the bulk gas if fueling is reduced sufficiently.

With this understanding that the smaller species arise predominantly from the outer boundary layer and/or bulk gas (depending on ϕ), it is interesting to compare the measured species with those predicted for incomplete bulk-gas combustion using a single-zone model and detailed iso-octane mechanism from LLNL [17], as discussed in the Introduction and reported in Ref. [3]. Of the four OHC species predicted by the model (formic acid, formaldehyde, acraldehyde, and acetaldehyde), all except formic acid were found in significant abundance. (Note that 2-propenal is another name for acraldehyde.) However, formic acid was not found in measurable quantities despite a specific effort to detect it. It is also noteworthy that acetone and 2-methyl-2-propenal were found in relative abundance, but were not noted in Ref. [3] as being main OHC emissions for incomplete bulk-gas combustion. An explanation for this may be found by examining Fig. 8, which shows that these species fall intermediate between the fuel and the light HC/OHC species. This indicates that they arise from the boundary layer where temperatures are cooler than in the bulk gas. Thus, in the single-zone computations, they should not be as prevalent as the smaller species unless ϕ is reduced so that combustion temperatures become lower than those at which the lighter HC/OHC emissions are dominant. The experimental data presented here also confirm that methane is the dominant bulk-gas HC emission as predicted by the single-zone model in Ref. [3].

Finally it should be noted that this explanation is based on an assumption that the temperature distribution remains similar to that shown in Fig. 9 throughout the combustion process. This should be correct to first order, since previous computational works based on KIVA/multi-zone modeling have shown generally good agreement with experimental data [13,14]. For these computations, mixture and temperature distributions are computed with KIVA up to the point of ignition, then frozen, while combustion behavior is computed using multi-zone kinetic modeling. Using this approach for computations in the current engine, at operating conditions similar to those of this study [14], showed distributions of fuel, intermediate HC and OHC, and CO that are in general agreement with the trends observed here. However, the actual in-cylinder processes are more complex, and a full CFD/kinetics computation would be required to fully resolve the effects of fluid motion and the temporal evolution of the combustion process. This has recently been completed and the detailed speciation measurements reported here are compared with these computational results in a concurrent study [19].

FUEL STRATIFICATION (SOI) SWEEP

As discussed in the introduction and shown in Figs. 1 and 3, the combustion efficiency becomes quite low for well-mixed HCCI as fueling is reduced to low loads. For an idle fueling rate of $\phi = 0.12$, the combustion efficiency is only 63% for the conditions presented in the previous section (Fig. 3), and HC and OHC emissions are high as discussed above. However, previous works [3,6,7] have demonstrated that stratifying the fuel/air mixture distribution can significantly improve combustion efficiency at low loads by raising the local equivalence ratios in the combustion chamber for the same total fueling rate.

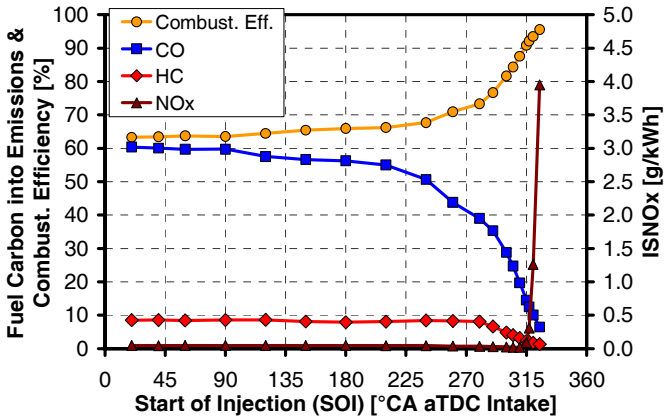

Figure 10. Combustion efficiency and global emissions as function of injection timing (SOI). 0°CA = TDC-intake and 360°CA = TDC-compression. ϕ = 0.12, T_{in} was adjusted to maintain CA50 = TDC throughout the sweep.

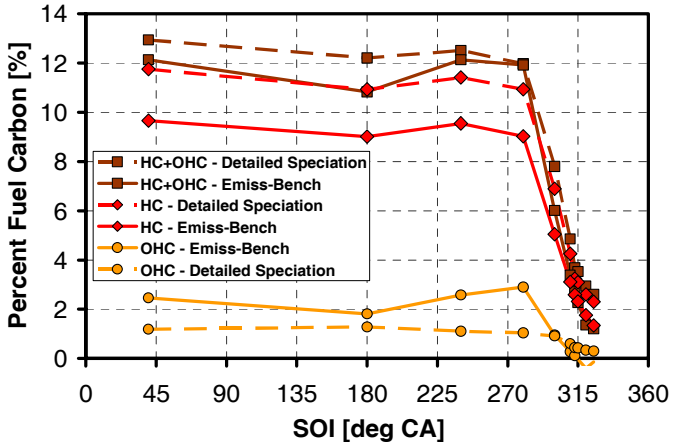

Figure 11. Comparison between the total HC, OHC, and HC+OHC emissions for conventional emissions-bench measurements (solid lines) and the sum of the detailed speciation (dashed lines).

Figure 10 shows how the combustion efficiency and global emissions change as the mixture is progressively stratified by delaying the start of injection (SOI) using an 8-hole GDI fuel injector. CA50 was maintained at TDC throughout this sweep by adjusting T_{in}, which varied between 200 and 212°C. Early injection gives essentially the same results as the premixed case shown in Fig. 3. As injection timing is delayed, there is no change until after 90°CA, at which point a slight downward trend in the CO begins. Then, beyond 210°CA CO levels fall more rapidly. The effect of stratification on the HC emissions is somewhat delayed, with a significant decline in HC not beginning until about 280°CA. Commensurate with these decreased emissions, the combustion efficiency increases, slowly at first and more sharply at the later SOIs. The reason for this improvement is that with a delayed SOI, the time for fuel/air mixing is reduced. This results in a local region of higher ϕ near the center of the combustion chamber [7] which burns hotter, enabling the bulk-gas reactions to reach completion. This trend of improving combustion efficiency continues for all SOIs investigated. However, for SOIs later than 315°CA, the mixture becomes sufficiently close to stoichiometric in some regions that NO_X emissions rise rapidly due to increased combustion temperatures. By 317°CA, they exceed the U.S. 2010 indicated specific NO_X ($ISNO_X$) limit of 0.27 g/kWh. Nonetheless, delaying the fuel injection increased the combustion efficiency from 63% for the well-mixed cases to 91% with NO_X levels still below the U.S. 2010 limits.

Comparison with Emissions-Bench Data – Because of the substantial potential of fuel stratification to improve low-load HCCI combustion, it is of interest to investigate its effects on the detailed speciation of the HC and OHC emissions. As first step in this process, Fig. 11 compares the sum of the HC, OHC, and HC+OHC emissions from the detailed speciation measurements against the emission-bench measurements that were acquired at the same time. Like the analogous plots for the equivalence-ratio sweep in Fig. 4, the total HC and OHC values from the detailed-speciation measurements in Fig. 11 have been adjusted to match the expected FID response of the emissions-bench measurements. Similar to the observations with the ϕ-sweep data (Fig. 4), the detailed-speciation measurements give about a 20% higher HC value and a lower OHC value than the emission-bench data, resulting in a slightly higher HC+OHC value for the detailed speciation data. However, unlike the ϕ-sweep data, the HC data for the two techniques in Fig. 11 track each other extremely well (albeit with an offset) giving confidence that the small dip in HC at 180°CA and the subsequent increase at 240°CA are real. Like the ϕ-sweep, the emission-bench OHC values were obtained by closing the carbon balance. As a result, they are somewhat noisy and are not considered to be very accurate. They will not be discussed further except to say that they match the general trend of the detailed-speciation data, showing little change in magnitude until about SOI = 280°CA and a substantial reduction in magnitude beyond this point.

Detailed-Speciation Data – For the starting point of this fuel-stratification sweep, the injection timing was in the early part of the intake stroke (40°CA). For this SOI, PLIF imaging [7] has shown that the charge is well mixed, and in agreement, engine performance and emissions data were shown to be almost identical to fully premixed operation [3,11]. The only difference noted was a very small (2%) increase in the HC measurement for the early direct injection case. In agreement, the emissions species identified here are the same species reported for the ϕ-sweep.

The main emissions are given in Fig. 12 along with the sums of the HC and OHC emissions for reference. As in the analogous plot for the ϕ sweep (Fig. 5), these totals have not been adjusted to match the FID response, but rather show the total of all carbons in the HC and OHC species. Therefore, the HC values are lower and the OHC values higher than in Fig. 11. Also, similar to the plots for the ϕ sweep, to facilitate distinguishing the

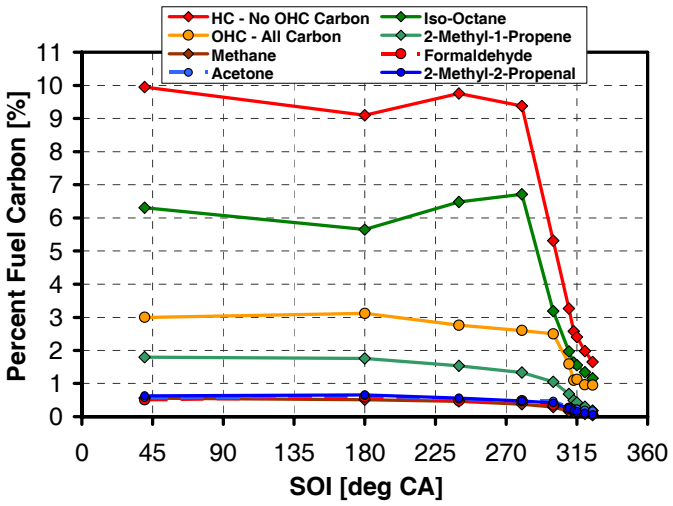

Figure 12. Main HC and OHC species as a function of start of injection (SOI). These HC and OHC curves are not adjusted to match FID data, but rather show the total of all the carbon in the HC and OHC species. The order of the species in the legend corresponds to their order at SOI = 180°CA, except for the last four species listed which nearly overlap.

curves of the various species when printing in black and white, the order of the species in the legend corresponds to the order of the species in the plot at the SOI given in the caption, for Figs. 12 - 16.

As can be seen in Fig. 12, unreacted fuel (iso-octane) is the most prevalent species. It is also noteworthy that the iso-octane curve shows a small dip at 180°CA, then rises again until 280°CA, before falling sharply to very low levels at the latest injection timings. This increase between 180 and 280°CA is not seen in the other species which generally show a more gradual decline beginning around 180°CA, followed by a sharper drop beyond 280°CA. This difference will be discussed in the next sub-section. As with the ϕ-sweep, the second most prevalent HC species is 2-methyl-1-propene, followed by methane. The methane curve closely overlaps the curves of the most prevalent OHC species, 2-methyl-2-propenal, formaldehyde, and acetone, when plotted on the scale used in Fig. 12.

Figure 13 shows the HC and OHC species that occur in lower quantities on an amplified scale, along with the species from Fig. 12 except iso-octane. Note that with this scaling, only the most stratified values of 2-methyl-1-propene are shown. As can be seen, the trends of these species generally match the trend of 2-methyl-1-propene described above, although some differences can be noted in the trends of a few species, which will be discussed later. Figure 14 shows the same data as Fig. 13, but with an expanded crank-angle scale.[3]

The main interest in stratified operation at this low fueling rate (ϕ = 0.12) is to improve the combustion efficiency as

[3] Note that although ethene was presented for the ϕ sweep, it is not presented here because of difficulties with the analysis.

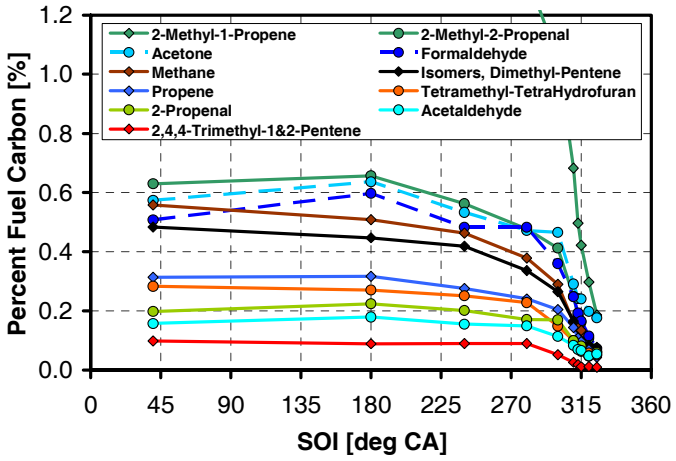

Figure 13. Lesser HC and OHC species as a function of start of injection (SOI). The order of the species in the legend corresponds to their order at SOI = 180°CA.

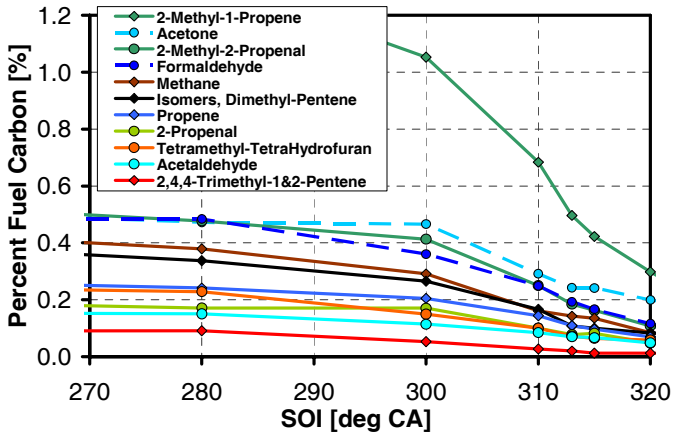

Figure 14. Lesser HC and OHC species as a function of SOI, with expanded SOI scale. The order of the species in the legend corresponds to their order at SOI = 300°CA.

much as possible. To accomplish this, it is desirable to operate at the latest injection timing while still maintaining acceptable NO_X emissions, as discussed above with respect to Fig. 10. This requires an SOI of about 315°CA for this case. Examining the trends in the HC and OHC emissions (Figs. 12 - 14) shows that as the SOI is delayed in the range of 315°CA, the emissions of all the species are declining rapidly. Small differences in the slopes of the various species cause some crossing of the curves (Fig. 14), but these effects are small compared to the overall decline. This shows that for the most part, the late injection timing is stratifying the charge as desired, creating a locally richer fuel/air mixture that burns hotter, and therefore, leaves less HC and OHC emissions.

The other factor causing a significant reduction in HC and OHC emissions is that with the reduced mixing time, less fuel reaches the crevices and the coldest boundary-layer region along the cylinder wall (see Fig. 9). This is particularly important for the large reduction in the amount of unreacted fuel (iso-octane), which comes

mainly from these regions where temperatures are very low, as discussed previously. As the SOI is retarded, iso-octane emissions fall from about 6% of the fuel carbon for well-mixed conditions to only 1.6% at SOI = 315°CA. This is substantially lower than even the 2.6% value for iso-octane emission at the highest load investigated with premixed fueling (ϕ = 0.28), where only fuel in the crevices is thought to remain intact [3]. Removing fuel from these coldest boundary-layer regions will also reduce the amount of other HC and OHC emissions, particularly the category-1 species that also require relatively cold temperatures.

However, when the mixture is stratified sufficiently so that there are regions with no fuel, there is always a gradient between the richer regions and the air in the rest of the cylinder. The portion of this mixture gradient with low equivalence ratios will result in HC and OHC emissions similar to those at the same ϕ in the premixed data presented previously. In fact, the outermost portions will have a lower ϕ than even the lowest shown for the ϕ sweep. In these regions, HC and OHC emissions will be very high on a percent fuel carbon basis, but not so high on an absolute basis since the amount of fuel is low. It should also be noted that this effect of low ϕ would be especially pronounced for the boundary-layer regions where the charge is cooler. For these reasons, there are still some HC and OHC emissions for even the most stratified cases, but their quantities are greatly reduced contributing (along with the CO reduction) to the large improvement in combustion efficiency. Finally, if the stratified-charge preparation technique could create a steeper mixture gradient from the richer regions to the surrounding air, these emissions would be further reduced with a corresponding improvement in combustion efficiency.

Differences in Trends for SOI = 180 - 300°CA – As noted above with the presentation of Figs. 12 and 13, some of the species show trends that are substantially different from the typical behavior. In particular, the iso-octane emissions in Fig. 12 show an increase from 180 - 280°CA that was not observed for any of the other species. Also, examination of Fig. 13 shows that the trends of at least four species are somewhat different from the general behavior. 2,4,4-trimethyl-1&2-pentene has almost a constant level until a sharp decline begins at 280°CA, and tetramethyl-tetrahydrofuran shows a lesser decline between 180 and 280°CA than the other species and has a sharper change of slope at 280°CA. In addition, some of the OHC species, particularly acetone and formaldehyde, show a slight increase at 180°CA prior to declining with greater stratification. These differences in the trends with stratification (SOI) are more evident when the emissions are normalized by their values for the well-mixed (early injection timing) case as shown in Figs. 15 and 16.

The initial drop in iso-octane at 180°CA and the subsequent increase from 180 - 280°CA are clearly evident in Fig. 15. As a check on the validity of these trends, Fig. 15a also shows the total HC from the emissions bench and the sum of the detailed-speciation measurements. These two independent measurements track each other extremely well, providing confidence in the total HC values. These total HC curves also show somewhat the same trend as iso-octane, since it is such a large con-

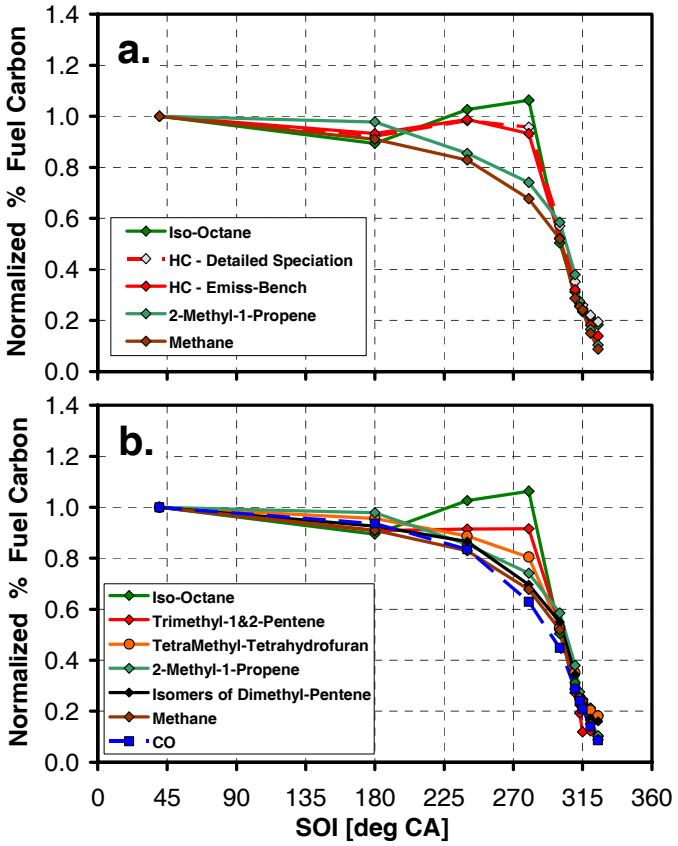

Figure 15. a) Normalized total HC, iso-octane and methane emissions and b) normalized iso-octane, other selected HC and OHC species, and CO as a function of SOI. The order of the species in the legend corresponds to their order at SOI = 280°CA.

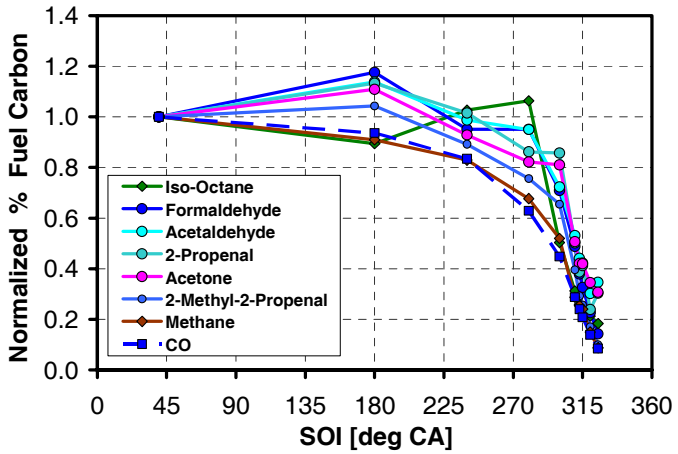

Figure 16. Normalized emissions of the main OHC species as a function of SOI. Iso-octane, methane and CO are also shown for reference. The order of the species in the legend corresponds to their order at SOI = 280°CA.

tributor to the total HC. However, for the total HC, the rise from 180 - 280°CA is somewhat reduced, compared to iso-octane, since most of the other HC do not show this increase, as indicated by the 2-methyl-1-propene and methane curves also shown in Fig. 15a. The initial drop in iso-octane can be explained by a little less fuel reaching the crevices as the SOI is delayed from 40 to 180°CA. The cause of the subsequent increase is less obvious, but the increase in unreacted fuel suggests that the amount of fuel reaching the crevices again increases. A possible explanation for this could be that as the piston moves up, it interacts with the fuel jets in such a way to either deflect the fuel toward the crevices, or allow the fuel jet to impinge more directly on the crevice. To help visualize this, Fig. 2c shows the nominal fuel-jet axes with respect to the piston at the 280°CA position. Although the jet axes do not align exactly with the entrance to the top ring-land crevice, they are close, and small changes in jet direction due to in-cylinder flows or jet-piston interactions could direct fuel into the crevice.

Assuming that for an SOI window around 280°CA more fuel enters the crevices, then a commensurate increase should also be noted in the category-1 HC species, which are formed by the least reaction from the parent fuel molecule. Figure 15b shows that this is, in fact, the case. In this normalized plot, 2,4,4-trimethyl-1&2-pentene shows higher values than the other HC species (expect iso-octane) in the 180 - 280°CA range, and this is followed by tetramethyl-tetrahydrofuran, which shows the next highest value. Thus, the progression in this SOI range from fuel to trimethyl-1&2-pentene to tetramethyl-tetrahydrofuran, to smaller species matches that observed in the ϕ sweep, as discussed previously. This provides further evidence of the validity of these trends.

Another anomalous behavior evident in Fig. 13 is that some of the OHC species showed an increase at about 180°CA before declining for later SOI. This trend is even more evident in the normalized plots presented in Fig. 16. As can be seen, emissions of the smaller (category-3) OHC compounds formaldehyde, acetaldehyde, 2-propenal, and acetone, increase by 18 – 11%, respectively, while the category-2 OHC, 2-methyl-2-propenal shows a more modest 4% increase.

This most likely results from the small amount of stratification produced by the 180°CA injection, which will make the mixture slightly richer in the central part of the combustion chamber and slightly leaner near the walls where temperatures are cooler. For the well-mixed case, these OHC species were most likely coming from the outer boundary layer, and not yet from the bulk gas at the fueling used here ϕ = 0.12. This statement is supported by the ϕ-sweep data in Fig. 8, which show that the emissions rate of these OHCs is still increasing as ϕ is reduced below 0.12, indicating that a greater portion of the charge mass contributes to their production. Thus, the richer mixtures near the center of the chamber do little to reduce the production of these OHC compounds, but the leaner mixtures in the cooler boundary layer cause more production. In contrast, the CO emissions for the well-mixed case are coming from almost the entire bulk gas, as evident by the fact that they remain nearly constant as ϕ is reduced below 0.12 (Fig. 3). Therefore, the slightly richer mixture, and hotter combustion, in the central part of the chamber reduces the CO production, in agreement with the drop noted in Fig. 16.

As discussed with respect to the ϕ-sweep data, full resolution of these trends would require detailed in-cylinder measurements and/or full CFD/kinetics modeling. However, as noted above, the main interest in stratification is to improve low-load combustion efficiency, so operation would primarily be with a later SOI (in the range of 315°CA) where the charge is much more stratified than in the SOI = 180 - 280°CA range.

SUMMARY AND CONCLUSIONS

Detailed exhaust speciation measurements have been made on an HCCI engine fueled with iso-octane over a range of fueling rates, and over a range of fuel-stratification levels. Fully premixed fueling was used for the fueling sweep. This sweep extended from a fuel/air equivalence ratio (ϕ) of 0.28, which is sufficiently high to achieve a combustion efficiency of 96%, down to a below-idle fueling rate of ϕ = 0.08 with a combustion efficiency of only 55%. The stratification sweep was conducted at an idle fueling rate (ϕ = 0.12) using an 8-hole GDI injector to vary stratification from well-mixed conditions for an early start of injection (SOI) (40°CA) to highly stratified conditions for an SOI well up the compression stroke (325°CA, 35°bTDC-compression). The engine speed was 1200 rpm for all measurements.

At each operating condition, samples were collected in Tedlar gas-sampling bags for analysis by GC-FID for the C1 and C2 hydrocarbon species and by GC-MS for all other species except formaldehyde and acetaldehyde. For these latter two species, a liquid-solution sampling technique was used and subsequent analysis performed using high-performance liquid chromatography (HPLC). In addition, standard emissions-bench exhaust analysis equipment was used to measure the total HC, CO, CO_2, O_2, and NO_X, simultaneously with the sampling for the detailed exhaust-species analysis. Good overall agreement was found between the emissions-bench data and the total HC from detailed-speciation measurements.

The study produced the following results:

1. The presence of significant quantities of oxygenated hydrocarbons (OHC) at low loads was confirmed, with formaldehyde, acetone, and 2-methyl-2-propenal being present in almost equal amounts, on a percent fuel carbon basis. Significant quantities of acetaldehyde, 2-propenal, and tetramethyl-tetrahydrofuran were also found.
2. Unreacted fuel, iso-octane, was by far the most prevalent hydrocarbon (HC) species for all fueling rates and stratification levels.
3. Numerous HC and OHC species were found that could be identified as breakdown products of iso-

octane (2,4,4-trimethyl-pentene, tetramethyl-tetrahydrofuran, dimethyl-pentene, 2-methyl-1-propene, and 2-methyl-2-propenal). In addition, several smaller species were identified, including the HC species methane, ethene, and propene, and the OHC species listed above.

4. The quantities of all HC and OHC species increased with reduced ϕ, but the trends in the rate of increase and the amount of emissions varied significantly between the various species.

5. Normalizing the emissions by their respective high-load values clearly shows the differences in their rates of increase with reduced ϕ, and these differences are shown to correlate well with the degree of molecular breakdown and reaction from the parent fuel toward complete combustion.

6. These trends in the normalized emissions can be explained, to first order, in terms of the expected in-cylinder temperature distribution. This analysis provides an indication of the in-cylinder location where the various species arise.

7. Reasonable agreement was found between the experimentally measured HC and OHC species arising from the bulk gas and those predicted by a single-zone model [3] using the LLNL iso-octane mechanism [17]. One exception was that the model predicted significant amounts of formic acid, which were not found experimentally.

8. For the SOI/stratification sweep, only small changes were found in the quantity of emissions of all species as injection was delayed from early in the intake stroke until over half-way up the compression stroke (280°CA). For SOIs beyond 280°CA, emissions of all HC and OHC species fell dramatically, in agreement with the improved combustion efficiency found previously for fuel stratification at low loads.

9. As the SOI was delayed beyond 280°CA, sharp reductions in iso-octane emissions, to levels below those found for high loads (on a percent fuel carbon basis), indicate that this improvement results from fuel no longer reaching the near-wall and crevice regions.

10. The data suggest that stratification increases combustion efficiency in two ways: 1) it produces a locally richer mixture in the central part of the charge which burns hotter and more completely (reducing emissions of CO and small HC and OHC species), and 2) the reduced mixing time removes fuel from the crevices and colder boundary-layer region near the cylinder wall, thus reducing the amount of unreacted fuel and larger HC and OHC species.

11. Further improvement of combustion efficiency at low loads could be achieved if stratified-charge mixture techniques were developed that produce steeper mixture gradients from the richer regions to the surrounding air, thereby reducing the size of the overly lean regions that produce OHC and HC under these conditions.

ACKNOWLEDGEMENTS

The authors would like to thank Leslie Carman of Lawrence Livermore National Laboratory for conducting the HPLC analysis, and the following people from Sandia National Laboratories for their help with this study: Kenneth St. Hilaire, Lloyd Claytor, and Eldon Porter for assembling and maintaining the engine; Christopher Carlen and Eldon Porter for help with the engine-control and safety-system electronics; and Gary Hubbard for help with the data acquisition system and programming support.

The engine experiments and gas sampling were performed at the Combustion Research Facility, Sandia National Laboratories, Livermore, CA. The detailed exhaust-speciation analysis was conducted at Lawrence Livermore National Laboratory, Livermore, CA. Support was provided by the U.S. Department of Energy, Office of FreedomCAR and Vehicle Technologies.

Sandia is a multiprogram laboratory operated by the Sandia Corporation, a Lockheed Martin Company, for the United States Department of Energy's National Nuclear Security Administration under contract DE-AC04-94AL85000.

The exhaust speciation analysis was performed under the auspices of the U.S. Department of Energy by Lawrence Livermore National Laboratory under Contract DE-AC52-07NA27344.

REFERENCES

1. Christensen, M., Johansson, B., and Einewall, P., “Homogeneous Charge Compression Ignition (HCCI) Using Iso-octane, Ethanol, Natural Gas – A Comparison with Spark Ignition,” SAE paper 972874, 1997.
2. Gray, A. W and Ryan, T. W., “Homogeneous Charge Compression Ignition (HCCI) of Diesel Fuel,” SAE paper 971676, 1997.
3. Dec, J. E. and Sjöberg, M., “A Parametric Study of HCCI Combustion – the Sources of Emissions at Low Loads and the Effects of GDI Fuel Injection,” SAE paper 2003-01-0752, 2003.
4. Sjöberg, M. and Dec, J. E., “Combined Effects of Fuel-Type and Engine Speed on Intake Temperature Requirements and Completeness of Bulk-Gas Reactions in an HCCI Engine,” SAE paper 2003-01-3173, 2003.
5. Sjöberg, M. and Dec, J. E., “An investigation into lowest acceptable combustion temperatures for hydrocarbon fuels in HCCI engines,” *Proc. Combust. Inst.,* Vol. 30, pp. 2719 – 2726, 2005.
6. Aroonsrisopon, P. W., Werner, P., Waldman, J. O., Sohm, V. and Foster, D. E., Morikawa, T., Minoru, I., “Expanding the HCCI Operation with the Charge Stratification,” SAE paper 2004-01-1756, 2004.
7. Hwang, W., Dec, J. E. and Sjöberg, M., “Fuel Stratification for Low-Load HCCI Combustion: Performance and Fuel-PLIF Measurements,” SAE paper 2007-01-4130, 2007.

8. Dec, J.E., “A Computational Study of the Effects of Low Fuel Loading and EGR on Heat Release Rates and Combustion Limits in HCCI Engines,” SAE paper 2002-01-1309, 2002.
9. Kaiser, E. W., Yang, J., Culp, T., Xu, N. and Marcq, M. M., “Homogeneous Charge Compression Ignition Engine-out Emissions – Does Flame Propagation Occur in Homogeneous Charge Compression Ignition?, *Int. J. Engine Research*, Vol. 3, No 4, pp. 185-195, 2002.
10. Iida, M., Foster, D. E., Hayashi, M., Martin, J. K., “Characteristics of Homogeneous Charge Compression Ignition (HCCI) Engine Operation for Variations in Compression Ratio, Speed, and Intake Temperature While Using *n*-Butane as a Fuel,” *ASME J. Gas Turbines and Power*, Vol. 124, 2002.
11. Dec, J. E. and Sjöberg, M., “Isolating the Effects of Fuel Chemistry on Combustion Phasing in an HCCI Engine and the Potential of Fuel Stratification for Ignition Control,” SAE paper 2004-01-0557, 2004.
12. Christensen, M., Johansson, B., and Hultqvist, A., “The Effect of Piston Topland Geometry on Emissions of Unburned Hydrocarbons from a Homogeneous Charge Compression Ignition (HCCI) Engine.” SAE paper 2001-01-1893, 2001.
13. Aceves, S. M., Flowers, D. L., Espinosa-Loza, F., Martinez-Frias, J., Dibble, R. W., Christensen, M., Johansson, B., and Hessel, R. P., “Piston-Liner Crevice Geometry Effect on HCCI Combustion by Multi-Zone Analysis,” SAE paper 2002-01-2869, 2002.
14. Aceves, S. M., Flowers, D. L., Espinosa-Loza, F., Martinez-Frias, J., Dec, J. E., Sjöberg, M., Dibble, R. W., and Hessel, R. P., “Spatial Analysis of Emissions Sources for HCCI Combustion at Low Loads Using a Multi-Zone Model,” SAE paper 2004-01-1910, 2004.
15. Jun, D. and Iida, N., “A Study of High Combustion Efficiency and Low CO Emission in a Natural Gas HCCI Engine,” SAE Paper 2004-01-1974, 2004.
16. Lemel, M., Hultqvist, A., Vressner, A., Hordgren, H. Persson, H., and Johansson, B., “Quantification of the Formaldehyde Emissions from Different HCCI Engines Running on a Range of Fuels,” SAE paper 2005-01-3724, 2005.
17. Curran, H. J., Gaffuri, P., Pitz, W. J., and Westbrook, C. K., “A Comprehensive Modeling Study of Iso-Octane Oxidation”, *Combustion and Flame*, Vol. 129, pp. 253 – 280, 2002.
www-cms.llnl.gov/combustion/combustion2.html
18. Kaiser, E. W., Marcq, M. M., Xu, N., Yang, J., “Detailed Hydrocarbon Species and Particulate Emissions from a HCCI Engine as a Function of Air-Fuel Ratio,” SAE paper 2005-01-3749, 2005.
19. Hessel, R P., Foster, D. E., Aceves, S. M., Davison, M. L., Espinosa-Losa, F., Flowers, D. L., Pitz, W. J., Dec, J. E., Sjöberg, M., and Babajimopoulos, A. “Modeling Iso-octane HCCI using CFD with Multi-zone Detailed Chemistry; Comparison to Detailed Speciation Data over a Range of Lean Equivalence Ratios,” SAE paper 2008-01-0047, 2008.
20. Heywood, J. B., Internal Combustion Engine Fundamentals, McGraw-Hill, New York, 1988.
21. Lipari, F. and Swarin, S. J., “Determination of Formaldehyde and Other Aldehydes in Automobile Exhaust with an Improved 2,4-dinitrophenylhydrazine Method,” *Journal of Chromatography*, 247, 297-306, 1982.

APPENDIX

	ϕ = 0.081			ϕ = 0.122			ϕ = 0.162			ϕ = 0.202			ϕ = 0.243			ϕ = 0.283		
	[ppm]	[%C]	[g/kg-fuel]	[ppm]	[%C]	[g/kg-fuel]	[ppm]	[%C]	[g/kg-fuel]	[ppm]	[%C]	[g/kg-fuel]	[ppm]	[%C]	[g/kg-fuel]	[ppm]	[%C]	[g/kg-fuel]
2,2,4-trimethylpentane (iso-octane)	108.40	8.025	80.252	118.270	5.858	58.583	116.840	4.353	43.533	129.170	3.869	38.693	133.380	3.337	33.370	122.160	2.627	26.272
2-methyl-1-propene	80.865	2.993	29.405	66.567	1.649	16.195	42.443	0.791	7.767	30.586	0.458	4.500	26.320	0.329	3.234	27.286	0.293	2.882
2-methyl-2-propenal	35.596	1.318	16.170	25.612	0.634	7.784	16.577	0.309	3.790	10.404	0.156	1.912	9.286	0.116	1.425	12.893	0.139	1.701
methane	125.40	1.160	13.038	88.200	0.546	6.136	30.000	0.140	1.570	12.200	0.046	0.513	9.700	0.030	0.341	8.400	0.023	0.254
formaldehyde	125.24	1.159	24.372	92.378	0.572	12.028	46.087	0.215	4.514	20.939	0.078	1.649	15.721	0.049	1.034	14.825	0.040	0.838
acetone	40.344	1.120	15.186	28.689	0.533	7.225	15.936	0.223	3.019	13.074	0.147	1.991	11.098	0.104	1.412	12.366	0.100	1.352
ethene	51.00	0.944	9.273	26.000	0.322	3.163	9.000	0.084	0.824	4.000	0.030	0.294	3.000	0.019	0.184	3.000	0.016	0.158
propene	22.00	0.611	6.000	16.000	0.297	2.920	8.000	0.112	1.098	5.000	0.056	0.552	5.000	0.047	0.461	4.000	0.032	0.317
2,2,4,4-tetramethyl-tetrahydrofuran	6.181	0.458	5.137	5.599	0.277	3.113	4.321	0.161	1.807	3.937	0.118	1.324	4.132	0.103	1.160	2.917	0.063	0.704
2-propenal	10.457	0.290	3.800	6.699	0.124	1.629	3.981	0.056	0.728	3.985	0.045	0.586	2.816	0.026	0.346	1.519	0.012	0.160
n-butyl ether	3.703	0.274	3.125	3.306	0.164	1.867	3.250	0.121	1.380	4.501	0.135	1.537	2.385	0.060	0.680	1.375	0.030	0.337
4,4-dimethyl-2-pentene	3.789	0.245	2.411	3.212	0.139	1.368	2.204	0.072	0.706	1.732	0.045	0.446	1.576	0.035	0.339	1.184	0.022	0.219
acetaldehyde	12.824	0.237	3.661	8.265	0.102	1.579	4.766	0.044	0.685	2.477	0.019	0.286	2.090	0.013	0.202	1.734	0.009	0.144
3-buten-2-one	5.847	0.216	2.656	3.312	0.082	1.007	2.308	0.043	0.528	1.949	0.029	0.358	1.738	0.022	0.267	0	0	0
1,3-butadiene	5.663	0.210	1.985	3.683	0.091	0.864	2.008	0.037	0.354	1.427	0.021	0.202	1.130	0.014	0.134	1.180	0.013	0.120
ethylene oxide	11.085	0.205	3.165	21.046	0.261	4.020	3.669	0.034	0.527	6.995	0.052	0.808	0	0	0	0	0	0
2,4-dimethyl-1-pentene	2.990	0.194	1.903	2.522	0.109	1.074	1.689	0.055	0.541	1.280	0.034	0.330	1.154	0.025	0.248	1.013	0.019	0.187
5-methylenenonane	2.093	0.194	1.899	1.910	0.118	1.159	2.168	0.101	0.990	3.179	0.119	1.167	1.202	0.038	0.369	0.618	0.017	0.163
2-methylpropanal	4.758	0.176	2.223	4.228	0.105	1.322	3.609	0.067	0.849	3.268	0.049	0.618	2.350	0.029	0.371	1.707	0.018	0.232
2,4-dimethyl-2-pentene	2.504	0.162	1.593	2.189	0.095	0.932	1.504	0.049	0.482	1.149	0.030	0.296	1.045	0.023	0.225	0.960	0.018	0.178
2-methyl-1-butene	3.034	0.140	1.379	2.696	0.083	0.820	1.733	0.040	0.396	2.644	0.050	0.486	2.379	0.037	0.365	2.068	0.028	0.273
2-methyl-1,3-butadiene	2.765	0.128	1.221	2.311	0.072	0.683	1.620	0.038	0.360	1.822	0.034	0.325	4.449	0.070	0.664	1.475	0.020	0.189
benzene	2.292	0.127	1.160	1.341	0.050	0.454	1.397	0.039	0.356	2.011	0.045	0.412	0.831	0.016	0.142	0.900	0.015	0.132
phenol	2.092	0.116	1.276	1.334	0.050	0.545	2.448	0.068	0.751	4.189	0.094	1.034	2.667	0.050	0.550	0	0	0
2,4,4-trimethyl-1-pentene	1.455	0.108	1.058	1.295	0.064	0.630	0.979	0.036	0.358	0.861	0.029	0.253	0.887	0.022	0.218	1.184	0.025	0.250
2,2-dimethyloxirane	2.479	0.092	1.158	1.422	0.035	0.445	1.428	0.027	0.336	0.524	0.008	0.099	1.315	0.016	0.208	0	0	0
2-propen-1-ol	3.071	0.085	1.156	2.123	0.039	0.535	1.324	0.018	0.251	0.650	0.007	0.099	0.926	0.009	0.118	0.783	0.006	0.086
2-butanone	1.710	0.063	0.799	1.713	0.042	0.536	1.894	0.035	0.445	1.394	0.021	0.264	1.241	0.016	0.196	3.613	0.039	0.491
2-butoxyethanol	1.076	0.060	0.824	0.518	0.019	0.265	1.066	0.030	0.411	1.027	0.023	0.318	0.839	0.016	0.217	0.980	0.016	0.218
toluene	0.734	0.048	0.438	0	0	0	0.494	0.016	0.149	1.273	0.033	0.308	0	0	0	0	0	0
ethane	2.000	0.037	0.390	2.000	0.025	0.261	1.000	0.009	0.098	0	0	0	0	0	0	0	0	0
2,4,4-trimethyl-2-pentene	0.489	0.036	0.356	0.402	0.020	0.196	0.315	0.012	0.115	0.260	0.008	0.076	0.266	0.007	0.065	0.228	0.005	0.048
2-methyl-1,3-pentadiene	0.560	0.031	0.298	0.457	0.017	0.163	0.419	0.012	0.112	0.538	0.012	0.116	0.225	0.004	0.041	0.192	0.003	0.030
4-methyl-1,3-pentadiene	0.535	0.030	0.285	0.442	0.016	0.158	0.430	0.012	0.115	0.503	0.011	0.108	0.201	0.004	0.036	0.229	0.004	0.035
1-butene	0.564	0.021	0.205	0.680	0.017	0.166	0.850	0.016	0.156	0.503	0.008	0.074	0.485	0.006	0.060	0.418	0.004	0.044
isomers, dimethyl-pentene (sum)	9.283	0.601	5.907	7.923	0.343	3.373	5.397	0.176	1.728	4.162	0.109	1.072	3.775	0.083	0.812	3.157	0.059	0.584
isomers, trimethyl-pentene (sum)	1.944	0.144	1.414	1.697	0.084	0.826	1.294	0.048	0.474	1.121	0.037	0.330	1.153	0.029	0.283	1.411	0.030	0.298

Table of all exhaust emission species measured for the equivalence-ratio sweep. Species are listed in order of the percent fuel carbon [%C] for the ϕ = 0.081 condition. Given at the bottom are the sums of the emissions of the three isomers of dimethyl-pentene (4,4-dimethyl-2-pentene + 2,4-dimethyl-1-pentene + 2,4-dimethyl-2-pentene) and the two isomers of trimethyl-pentene (2,4,4-trimethyl-1-pentene + 2,2,4-trimethyl-2-pentene), as presented in Figs. 6 and 8.